Hindawi
Shock and Vibration
Volume 2021, Article ID 5022711, 17 pages
https://doi.org/10.1155/2021/5022711

Research Article

Performance Degradation of Subsea Shield Tunnel Segment Accounting for Concrete Strength Loss and Steel Bar Corrosion

Jiaqi Guo,[1] **Weiling Yang**,[1] **Chong Xu**,[2] **Bo Peng**,[1] **Jinhai Lin**,[2] **and Yuan Qian**[1]

[1]*School of Civil Engineering, Henan Polytechnic University, Jiaozuo 454003, China*
[2]*China Railway First Survey and Design Institute Group Co., Ltd., Xi'an 710043, China*

Correspondence should be addressed to Chong Xu; 14319984@qq.com

Received 15 August 2021; Accepted 27 October 2021; Published 24 November 2021

Academic Editor: Yujing Jiang

Subsea shield tunnels usually serve in a typical corrosive marine environment. Under the action of chloride penetration and carbonization, tunnel lining segments are often damaged because of concrete strength loss and steel bar corrosion induced concrete cracking during their service life, which seriously degrades the service performance of the tunnels. A systematical experimental and numerical investigation into the performance degradation of subsea shield tunnel segments accounting for concrete strength loss and steel bar corrosion is presented in this paper. The study demonstrates that chloride penetration decreases the peak strength and elastic modulus of the segment concrete by 42% and 46.1%, respectively. The average of the ratio of dissipated energy to the total energy of dry concrete is much smaller than that of water saturated concrete and chlorine solution saturated concrete, and chloride penetration reduces the energy storage capacity of concrete, and the ability to resist damage is weakened. When steel bars corrode for 120 days, the outer cracks continue to extend, and the concrete around the inner steel bars just begin to crack initiation; when corrode for 20 years, the length of the inner cracks gradually exceeds that of the outer cracks, and the inner cracks initiating from different steel bars coalesce with each other and form a continuous failure surface, causing great serious damage to the segment. Due to the difference in concrete strength, for the outer layer, the evolution processes of steel bar corrosion-induced cracks show the characteristics of early initiation, slow propagation, and late coalescence, and those for the inner layer have the characteristics of late initiation, rapid propagation, and early coalescence. During the whole process the propagation speed of the inner and outer cracks appears to be fast first and then slow. Moreover, the study also illustrates that the final state of segment performance degradation after crack coalescence presents the characteristics of whole lamellar exfoliation of the concrete cover.

1. Introduction

Shield tunneling has become a widely used construction method for subsea tunnels due to its strong adaptability to geological conditions, quick and safe construction, and low water inrush and collapse on the tunnel face [1]. Because of the high salinity and high seepage pressure of seawater, the outer surface of the lining segments of the subsea shield tunnel is continuously exposed to the corrosive environment of seawater. The chloride in seawater (shown in Figure 1), on the one hand, penetrates from the outside to the inside of the segment by means of perennial unsaturated seepage of seawater, which reduces the strength of the segment concrete by crystallizable-degradable corrosion. In addition, the chloride that has penetrated into the segment will enrich around the steel bars and result in the steel bars to rust while the critical chloride concentration is reached, which produces corrosion products 2 to 4 times the corresponding volume of the steel bar, causing corrosion-induced concrete cracking [2–4]. For the inner surface of the lining segment, due to the closed environment in tunnels, the high concentration of carbon dioxide in the air coming from dense crowd and vehicle exhaust gas will carbonize the segment concrete as illustrated in Figure 1. Although carbonization does not reduce the concrete strength, it weakens the alkalinity of the concrete to activate the steel bar passivation film and also causes corrosion-induced concrete cracking [2]. These degradation behaviors are the main inducements

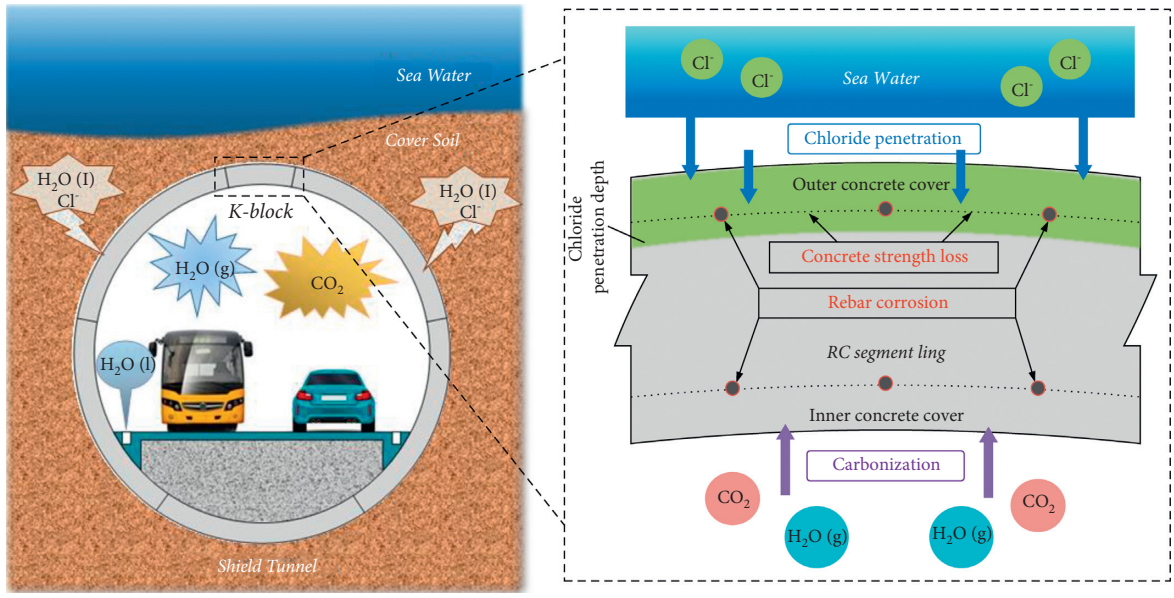

FIGURE 1: Typical working environment of subsea shield tunnel: (a) shield tunnel lining segments in the subsea corrosive environment and (b) performance degradation mechanism of lining segment.

for durability damage of lining segments of subsea shield tunnels and will seriously affect their normal service. Because of the complexity of subsea geological conditions and the strong concealment of the tunnels, it is difficult to make a major repair for durability damage after tunnel construction completion. Therefore, it is of great significance to figure out the evolutionary properties of performance degradation of subsea shield tunnels to support their service performance evaluation and repair.

A great deal of researches have been carried out worldwide concerning the degradation behavior of subsea shield tunnels. Abbas and Nehdi [5] explored the degradation mechanism of specimens extracted from full-scale segments subjected to chloride ion exposure and investigated the flexural strength of the segments. Yin et al. [6] investigated the degradation of mechanical properties of shield tunnel segments by testing the bearing capacities under the effect of water permeation and salt environment of chloride. Kong et al. [7] used the strength reduction method to reduce the strength parameters of segment concrete after chloride penetration and researched the influence of chloride penetration on the deformation characteristic of subsea shield tunnels. Lei et al. [8] conducted durability tests on shield segment specimens under the coupling effect of load and chloride environment, with which the influence of environmental chloride concentration on the mechanical properties of the segments is summarized. Bao et al. [9] analyzed and summarized the law of chloride ion erosion under marine exposure environment and, from the perspective of marine exposure test and indoor simulation test, summarized the research progress of chloride ion erosion resistance of environmental concrete in the marine tidal zone. With further in-depth studies, researchers realized that only focusing on chloride-induced mechanical degradation of segment concrete is not enough. The corrosive environment (including chloride penetration, carbonization, etc.) caused steel bar corrosion may bring greater durability damage to the segment and should take into consideration. Many researches have been conducted concerning steel bar corrosion and related final failure state. Feng et al. [10] investigated the characteristics of steel bar corrosion-induced concrete cracks in the lining segments and the time-variant failure probability of shield tunnels in a marine environment by corrosion-accelerated experiments on individual segments. He et al. [11] studied the corrosion characteristics of steel bars in shield tunnel concrete segment and observed the damage pattern of corroded segment surface. Li et al. [12] carried out the mechanical tests on a set of segment components with different corrosion degrees to study the performance degradation law of shield tunnel lining structure under chloride penetration. Li et al. [13] acquired the durability and degradation features of shield tunnel concrete segments under the joint action of chloride salt, carbonation, and other corrosion environment factors by conducting accelerated environmental and direct current power simulation tests. Li et al. [14] studied the performance degradation of tunnel lining structure under the action of steel corrosion and considered that arch foot and vault were more sensitive to steel corrosion.

The existing research achievements have played a significant role in promoting the study on durability performance degradation of subsea shield tunnels. However, they only focus on a single degradation behavior between concrete strength loss and steel bar corrosion-induced concrete cracking, and few explorations consider the combined action of both. Actually, a segment can be divided into the inner and outer layers according to the chloride penetration depth. For the inner layer, since

carbonization does not reduce the strength of the concrete, we can only consider steel bar corrosion-induced concrete cracking; while for the outer layer, before the steel bar corrosion, chloride penetration has led the outer layer concrete to lose some strength. Therefore, the durability damage of the outer layer is caused by the combined action of concrete strength loss and steel bar corrosion-induced concrete cracking. For this reason, this study intends to make some explorations on the time-variant durability damage evolution process and performance degradation characteristics of the lining segment of subsea shield tunnel with considering concrete strength loss and steel bar corrosion-induced concrete cracking. This paper is based on the conventional triaxial compression tests; the strength, deformation, and energy evolution characteristics of segment concrete under seawater erosion were analyzed from the mechanical and energy perspectives. Then, based on the strength and deformation parameters acquired from the above test, the performance degradation process and corresponding characteristics of the lining segment were studied by a series of numerical simulations; it has certain guiding significance for the study of the durability of submarine shield tunnels and provides a certain reference for future related research.

2. Mechanical Behavior and Energy Properties of Chloride-Penetrated Segment Concrete

2.1. Preparation of Concrete Samples and Testing Procedure. Segment concrete strength loss is mainly due to the infiltration of seawater. On the one hand, the seawater seepage gradually saturates the concrete; then the liquid water in the micropores exerts extrusion pressure on the wall of the pores under the action of external force, which causes the cracks to expand and the strength of the concrete to reduce. In addition, the corrosive action of chloride ions carried by seawater will also cause its strength to be further reduced. Therefore, dry concrete samples (group A), water saturated concrete samples (group B), and chloride solution saturated concrete samples (group C) are prepared. Through conducting triaxial compression tests on these samples, the strength and deformation characteristics are compared, and the strength weakening caused by the seawater corrosion of the segment concrete is discussed.

The samples in the test are processed from the C50 concrete test cube provided by the shield tunnel segment supplier. After drilling, sampling, and polishing, the cylindrical standard samples with a diameter of 50 mm and a height of 100 mm are acquired, as shown in Figure 2(a). In order to reflect the difference in the corrosion state of the concrete located in different parts of the segment during service, the three groups of samples A, B, and C are pretreated in different ways, and the details are shown in Table 1. Afterwards, the shear wave velocity of each group of samples are tested, and the samples with similar wave velocity are selected to reduce the errors caused by inner defects and incomplete pretreatment.

Five samples from each group are taken to subject to conventional triaxial compression test on the RMT-150B rock mechanics electro-hydraulic servo test system (as shown in Figure 2(c)). The design confining pressures are five stress levels of 2 MPa, 4 MPa, 6 MPa, 8 MPa, and 10 MPa. During the test, the confining pressure is controlled by stress and loaded to the design values at a rate of 0.100 MPa/s to keep the samples in an approximate static equilibrium state. Then, the confining pressure is kept unchanged, and the displacement control mode is used to continuously apply an axial load to the samples at a rate of 0.0020 mm/s until samples fail. The damaged samples after triaxial compression are shown in Figure 2(d). In the process, the complete stress-strain curves are obtained, and based on them, the peak strength and elastic modulus are calculated.

2.2. Strength and Deformation Characteristic of the Segment Concrete Samples. After triaxial compression, the stress-strain curves of the samples are obtained, as shown in Figure 3.

It can be seen from Figure 3 that under triaxial compression, the samples have experienced pore fracture compaction stage, elastic deformation stage, transition stage, and failure stage. When the samples are close to the peak, the curves drop gently; the stress drop is not obvious; and the plasticity and ductility characteristics are very obvious. Moreover, the plasticity and ductility become more and more obvious with the increase of confining pressure, and the samples gradually transit from elastic brittleness to elastic-plastic. The elastic limit of the samples in each group also increased significantly with the increase of confining pressure, and the peak strength and peak strain also increased significantly with the increase of confining pressure.

In order to more intuitively analyze the influence of chloride solution on the strength weakening of concrete materials, the peak strength is extracted from Figures 3(a)~3(c), and the results are illustrated in Figure 4. With the increase of confining pressure, the peak strength of the samples in each group increased significantly from Figure 4, reflecting prominent pressure induration. Generally, the strength characteristics of concrete can be described by the Coulomb criterion. This criterion, expressed by principal stress, can be expressed as $\sigma_1 = f_c + k\sigma_3$ (f_c is the uniaxial compressive strength of concrete and k is the strength parameter associated with the material), which represents the relationship between the peak strength and the confining pressure for a specific concrete sample. Figure 4 illustrates the regression relationship and correlation coefficients of peak strength and confining pressure of the samples in each group according to the Coulomb criterion. From the values of correlation coefficient R, it can be concluded that the peak strength of seawater uncorroded concrete, water saturated concrete, and chlorine-corroded saturated concrete has a favorable linear relationship with confining pressure, which follows the Coulomb criterion.

Figure 4 reflects the obvious difference in peak strength of the samples with different corrosion states under the same confining pressure. To accurately reflect the weakening effect

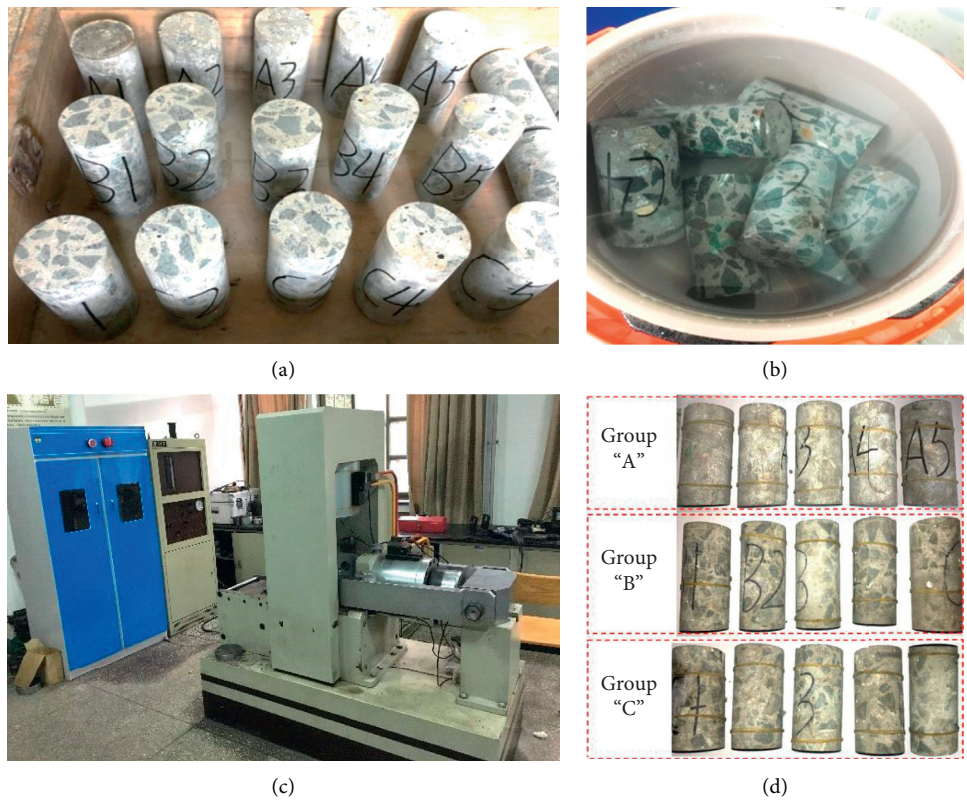

Figure 2: The procedure of triaxial compression test: (a) concrete samples, (b) soaking the samples in an electric cooker, (c) RMT-150B test system, and (d) samples after mechanical tests.

Table 1: The pretreatment methods for the three groups of concrete samples.

Groups of samples	Simulation object	Pretreatment method	Specific pretreatment processes
Group A	Uncorroded concrete	No treatment	None
Group B	Water saturated concrete	Soaking in warm pure water	Place the samples in an electric cooker filled with pure water, keep the water temperature at 60°C, and continue soaking for 24 hours to fully saturate the concrete samples
Group C	Chlorine-corroded saturated concrete	Soaking in warm chloride solution	Place the samples in an electric cooker filled with 2.5% NaCl solution, keep the water temperature at 60°C, and continue soaking for 24 hours to fully saturate the samples and ensure the chloride fully penetrates into the concrete, as demonstrated in Figure 2(b)

of chloride solution on the strength of the segment concrete, Table 2 compares the peak strength and elastic modulus of the three groups of samples. According to Table 2, it can be found that the average ration of the peak strength of group B to group A is 64.0% and that of group C to group A is 58.0%, which indicates that the seepage of water significantly reduces the strength of segment concrete by 36%. The corrosion of chloride ions after water saturated further reduces the strength by 6%.

By comparing the elastic modulus of the samples in different groups, the influence of chloride penetration on the deformation characteristics of the segment concrete is obtained. As demonstrated in Table 2, the elastic modulus of group B is significantly lower than that of group A. The average value of elastic modulus reduced from 38.928 GPa to 22.322 GPa, and for group C, it further reduced to 20.967 GPa. The elastic modulus of the two groups is 57.3% and 53.9% of group A, respectively, indicating that water seepage and chloride penetration significantly reduced the elastic modulus of the segment concrete.

As previously mentioned, taking the seawater corrosion depth as the boundary, a segment can be divided into the inner and outer layers. The above test results indicate that the strength and elastic modulus of the outer layer of the segment concrete are greatly reduced compared with the inner layer due to seawater corrosion. Therefore, the weakening effect of seawater corrosion on the strength of segment concrete should be considered in the performance degradation analysis of subsea shield tunnels. The performance deterioration of segment concrete caused by seawater

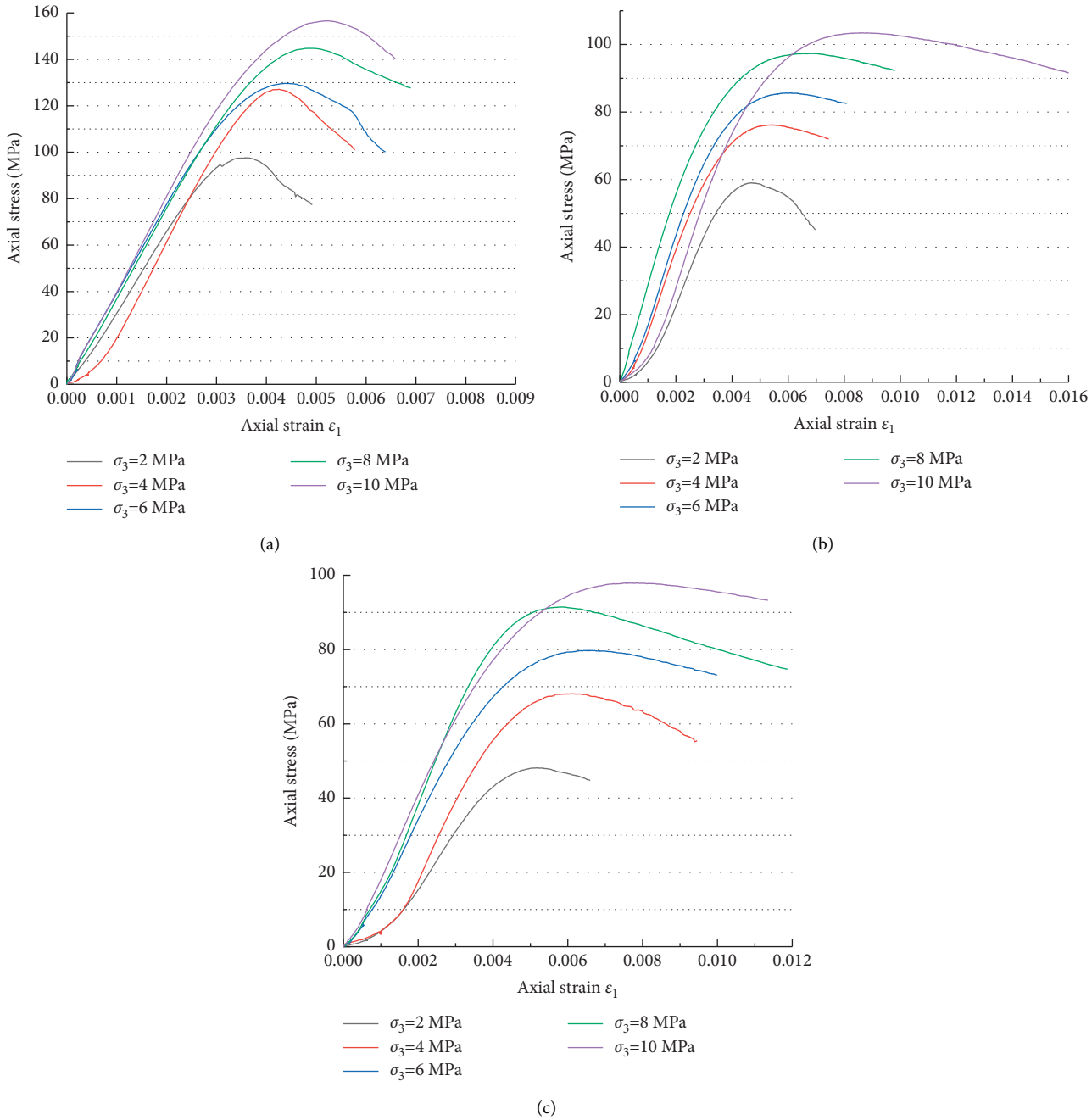

Figure 3: Stress-strain curves of samples under triaxial compression: (a) group A samples under triaxial compression, (b) group B samples under triaxial compression, and (c) group C samples under triaxial compression.

erosion cannot be ignored in the durability analysis of subsea tunnels.

2.3. Analysis of Segment Concrete Material Deterioration Based on Energy Perspective. The change law of material failure energy based on thermodynamics is more beneficial to reflect the essential characteristics of rock strength change and overall failure under external load [15]. Therefore, based on the energy perspective, this section will study the energy evolution process in the failure process of dry concrete that has not been eroded by seawater and saturated concrete that has been eroded by seawater and reveal the influence mechanism of seawater on the performance degradation of segment concrete.

Rock units were studied when doing energy analysis, which deformed under outer force, and this process can be supposed to be no heating exchanges. Based on the conservation of energy, the total input work U would be [15]

$$U = U^d + U^e, \tag{1}$$

where U^d is dissipated energy and U^e is releasable elastic strain energy.

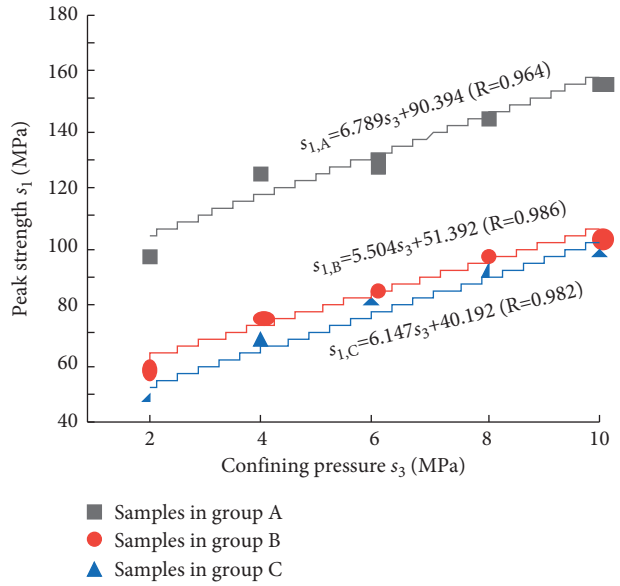

Figure 4: Relationship between peak strength and confining pressure of the three group samples.

As shown in Figure 5, areas in shadow are the releasable elastic strain energy U^e stored in the rock unit. The areas between unloading elastic modulus E_i and stress-strain curve are dissipated energy U^d, which represents the energy dissipated by the internal damage and plastic deformation in the process of loading.

Under complex stress state, the energy of each part of concrete specimen in principal stress space can be expressed as follows:

$$U = \int_0^{\varepsilon_1} \sigma_1 d\varepsilon_1 + \int_0^{\varepsilon_2} \sigma_2 d\varepsilon_2 + \int_0^{\varepsilon_3} \sigma_3 d\varepsilon_3, \tag{2}$$

$$\begin{aligned} U^e &= \frac{1}{2E_i}\left[\sigma_1^2 + \sigma_2^2 + \sigma_3^2 - 2\mu\left(\sigma_1\sigma_2 + \sigma_2\sigma_3 + \sigma_1\sigma_3\right)\right] \\ &\approx \frac{1}{2E_0}\left[\sigma_1^2 + \sigma_2^2 + \sigma_3^2 - 2\mu\left(\sigma_1\sigma_2 + \sigma_2\sigma_3 + \sigma_1\sigma_3\right)\right], \end{aligned} \tag{3}$$

$$U^d = U - U^e, \tag{4}$$

where E_0 is the initial elastic modulus of the sample; μ is the Poisson ration; σ_1, σ_2, and σ_3 are the stress in the main stress direction, ε_1, ε_2, and ε_3 are the elastic strain in the direction of main stress.

For conventional triaxial compression, $\sigma_2 = \sigma_3$, $\varepsilon_2 = \varepsilon_3$, equations (2)~(4) can be written as follows:

$$\begin{aligned} U &= \int_0^{\varepsilon_1} \sigma_1 d\varepsilon_1 + 2\int_0^{\varepsilon_3} \sigma_3 d\varepsilon_3, \\ U^e &= \frac{1}{2E_i}\left[\sigma_1^2 + 2\sigma_3^2 - 2\mu\left(\sigma_3^2 + 2\sigma_1\sigma_3\right)\right] \approx \frac{1}{2E_0}\left[\sigma_1^2 + 2\sigma_3^2 - 2\mu\left(\sigma_3^2 + 2\sigma_1\sigma_3\right)\right], \\ U^d &= \int_0^{\varepsilon_1} \sigma_1 d\varepsilon_1 + 2\int_0^{\varepsilon_3} \sigma_3 d\varepsilon_3 - \frac{1}{2E_0}\left[\sigma_1^2 + 2\sigma_3^2 - 2\mu\left(\sigma_3^2 + 2\sigma_1\sigma_3\right)\right]. \end{aligned} \tag{5}$$

According to the above relationship, the test data of group A, group B and group C concrete samples under triaxial compression were processed, and the energy evolution curves of group A, group B and group C samples during the failure process were obtained. Take confining pressure 4 MPa and 8 MPa for example, as shown in Figure 6.

As shown in Figure 6, each sample has similar energy evolution characteristics in triaxial compression. The failure process of the samples is divided into four stages: compaction stage, linear elastic stage, transition stage, and failure stage. The increase and decrease trend of energy in each stage is relatively consistent. The total energy U increases from compression to destruction, and this process absorbs energy

Table 2: Comparison of triaxial compressive strength and elastic modulus of the three groups of samples.

σ_3 (MPa)	$\sigma_{1,A}$ (MPa)	$\sigma_{1,B}$ (MPa)	$\sigma_{1,C}$ (MPa)	$\sigma_{1,B}/\sigma_{1,A}$	$\sigma_{1,C}/\sigma_{1,A}$	$\sigma_{1,B}/\sigma_{1,C}$	E_A (GPa)	E_B (GPa)	E_C (GPa)
2	97.53	59.018	48.139	0.605	0.494	0.816	34.980	20.783	19.678
4	127.101	76.211	68.091	0.600	0.536	0.893	41.487	22.222	21.721
6	129.657	85.695	79.746	0.661	0.615	0.931	37.474	23.607	20.763
8	144.765	97.361	91.457	0.673	0.632	0.939	40.990	23.434	20.758
10	156.588	103.484	97.921	0.661	0.625	0.946	39.709	21.614	20.624
Average value	—	—	—	0.640	0.580	0.905	38.928	22.332	20.709

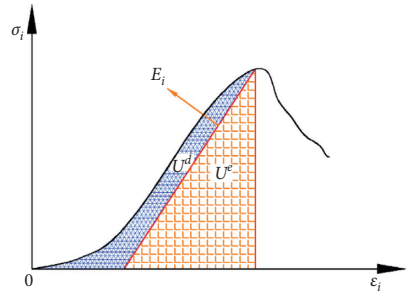

Figure 5: Relationship curve between dissipated energy and releasable strain energy of rock [16].

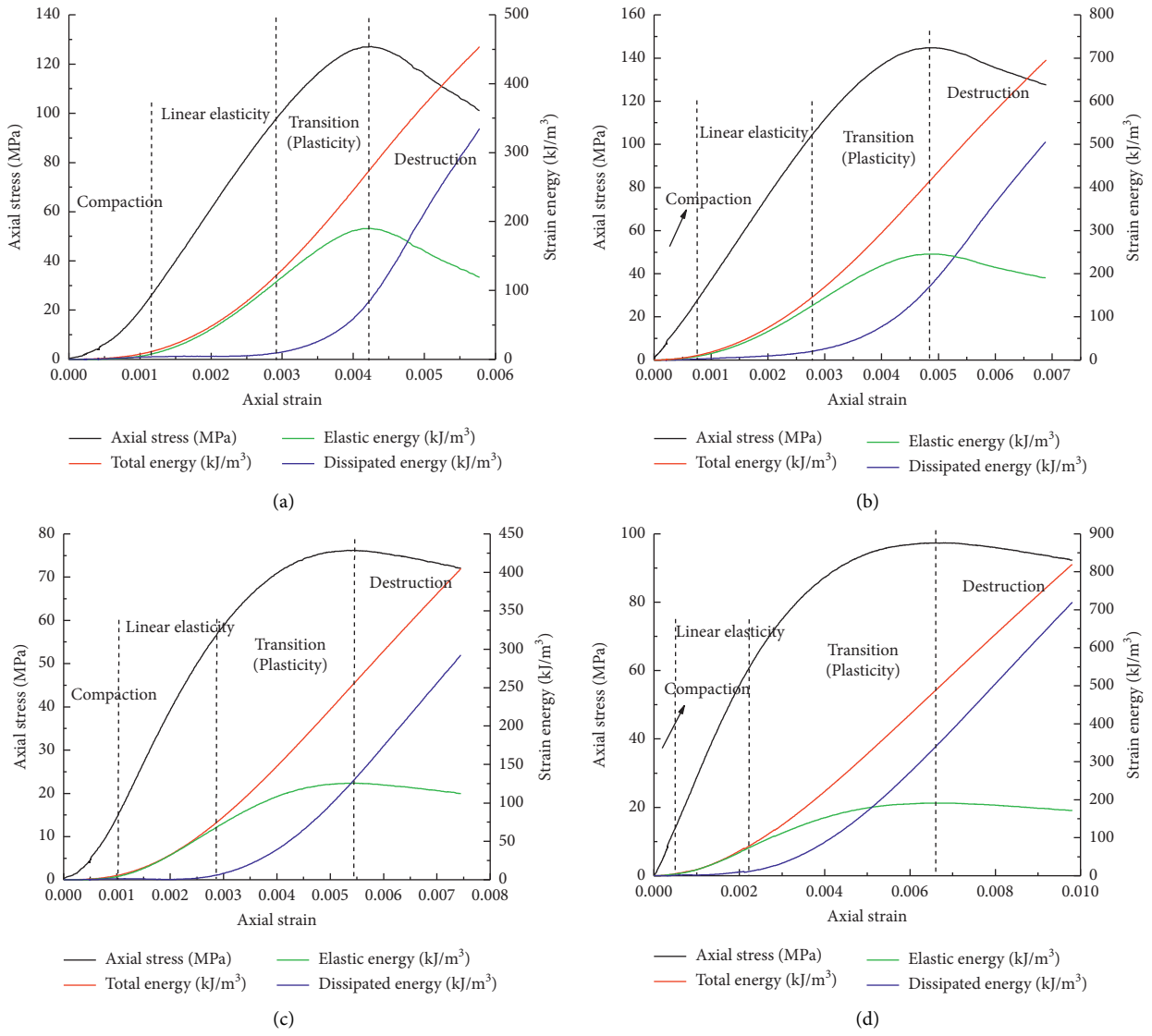

Figure 6: Continued.

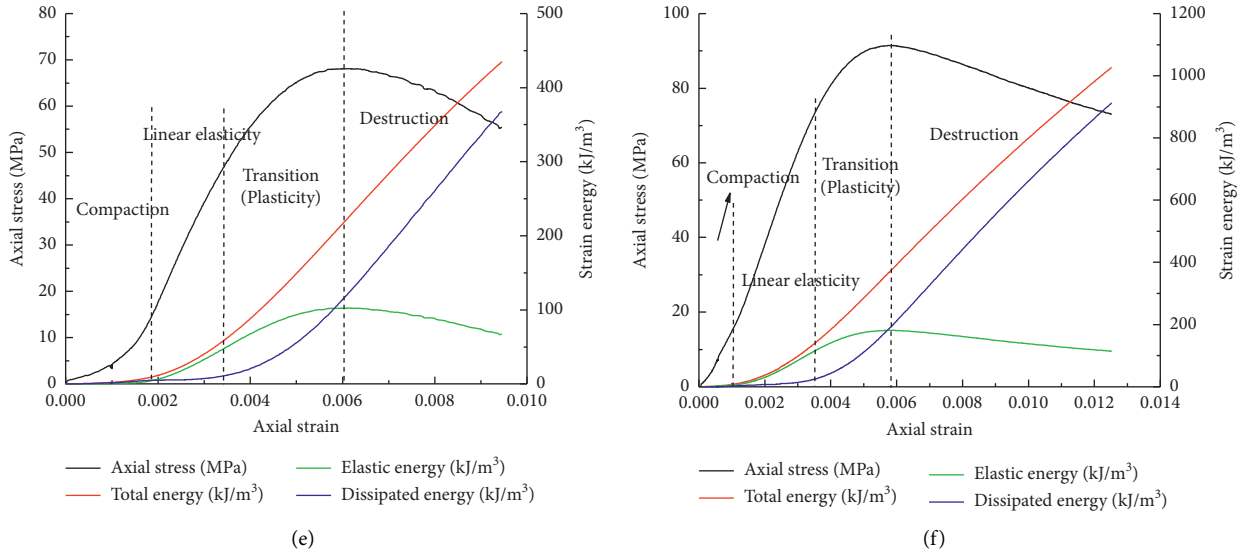

Figure 6: The relationship between strain energy and axial strain under different confining pressures: (a) group A samples under 4 MPa confining pressure, (b) group A samples under 8 MPa confining pressure, (c) group B samples under 4 MPa confining pressure, (d) group B samples under 8 MPa confining pressure, (e) group C samples under 4 MPa confining pressure, and (f) group C samples under 8 MPa confining pressure.

from the outside; The dissipated energy U^d increases very little in compression and linear elastic stage and increases rapidly in the transition and failure stages. The elastic energy U^e increases first, reaches the maximum at the peak strength, and then decreases gradually, indicating that the elastic energy of the sample accumulates first and then releases in the process of triaxial compression. With the increase of confining pressure, the increase rate of elastic strain energy decreases, while the increase rate of dissipated energy increases.

In order to analyze conveniently the difference of energy evolution among dry concrete (group A), water saturated concrete (group B), and chlorine solution saturated concrete (group C), the strain energy at the peak of each group of samples was extracted, and the ratio of dissipated energy to the total energy (U^d/U) at the peak stress point and its average value were calculated; the relationship between samples U^d/U and confining pressure is shown in Figure 7. The average U^d/U of group A is 0.39; the average U^d/U of group B is 0.54; and the average U^d/U of group C is 0.55.

As shown in Figure 7, the average U^d/U of group A is much smaller than that of groups B and C; the average U^d/U of group B and C is relatively close; the average U^d/U of group B was 1.38 times that of group A; and the average U^d/U of group C was 1.41 times that of group A. Dissipative energy is the essential property of deformation and failure of concrete samples; its process is unidirectional and irreversible; this part of the strain energy dissipates in the form of plastic damage deformation energy and crack propagation fracture surface energy in the closed friction of primary defects, the initiation and evolution of new microcracks, the macro cracks formation, and plastic deformation in the samples; it runs through the compaction stage, the stable growth of microcracks, the accelerated growth of cracks, and

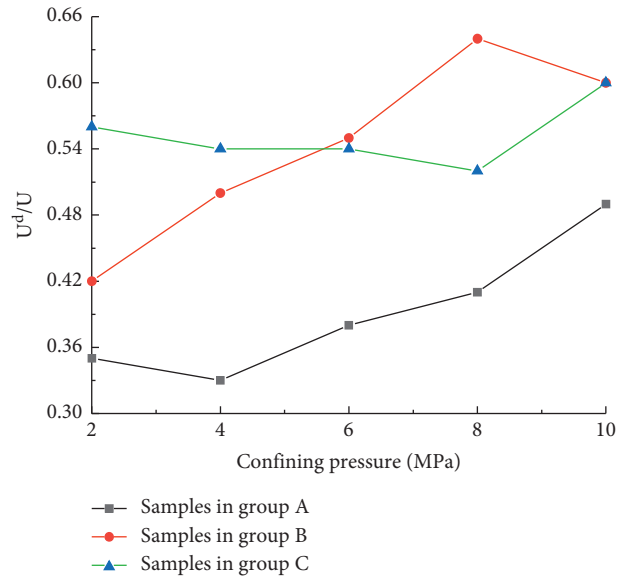

Figure 7: Curve of the samples U^d/U changing with confining pressure at the peak stress point.

even the elastic stage in the deformation process of the samples; therefore, it can be considered that the larger the proportion of dissipated energy, the more serious the crack initiation, diffusion, and plastic deformation when the peak stress is reached, the worse the energy storage capacity of concrete, the weaker the ability of the samples to resist failure, and the more prone to failure under the same stress level. In conclusion, it can be concluded that seawater erosion has a significant degradation effect on segment concrete materials; under the same stress level, the cracks of concrete in seawater environments are more likely to initiate and expand faster, and the bearing capacity is weaker.

It is difficult to find the difference of energy characteristics between group B and group C samples from the average U^d/U, and the difference can be revealed from the peak total energy and elastic energy of the samples. Figure 8 is the curves of total energy and elastic energy of group B and group C samples with confining pressure at the peak stress point; it can be found that the total energy of group B samples is slightly larger than that of group C samples under different confining pressures, indicating that the total work of seawater saturated samples can withstand the outside world before failure is less than that of water saturated samples, as shown in Figure 8(a). It can also be observed that the elastic strain energy of the samples in group B is also slightly larger than that in group C, as shown in Figure 8(b), and only when the elastic deformation in the unit can reach the surface energy required for damage, the unit body can be destroyed by the release of strain energy [15]. Therefore, the surface energy required for the destruction of seawater saturated samples is slightly smaller, and the easier it is to achieve, the easier it is to destroy; it reveals the reason why the strength and elastic modulus of seawater saturated samples are slightly smaller than those of tap water saturated samples.

3. Performance Degradation Evolution of Subsea Shield Tunnel through Numerical Investigation

In the second section, based on the conventional triaxial compression tests, the mechanical properties and energy characteristics of segment concrete under dry state, water saturation state, and chloride solution saturation state are studied from the aspects of strength, elastic modulus, stress-strain relationship, and energy characteristics, and the influence mechanism of seawater erosion on the performance degradation of segment concrete is revealed. At the same time, the results of the above section provide relevant parameters for the numerical simulation of this section. However, the above researches are insufficient, which are not enough to study the performance degradation evolution of subsea shield tunnel. In this section, the corrosion cracking, damage degradation characteristics, and performance degradation process of subsea tunnel segments are systematically studied by numerical simulation method.

3.1. Program for Numerical Simulation for Performance Degradation. At the beginning of the service of subsea shield tunnel, chloride was transported from the outside of the segment to the inside through convection and diffusion with the seawater as a carrier until the chloride enriched on the surface of the outer steel bars reached the critical concentration; then the outer steel bars began to rust [17]. For the inner steel bars, under the action of carbonization, when the pH value of the concrete around the steel bars decreases to the critical value, rust also begins [2]. Previous studies have found that it takes about 34.6 years for the former and about 38.8 years for the latter [18]. Considering the most unfavorable state conservatively takes the smaller value namely 34.6 years as the beginning time of steel bar corrosion for the tunnel, and at that time, the depth of chloride penetration into the segment is about 100 mm [18]. In this paper, the K-block segment (dimension is shown in Table 3) in the above state is taken to analyze the time-variant durability damage and performance degradation of lining segments accounting for concrete strength loss and steel bar corrosion. According to the chloride penetration depth when serving for 34.6 years, the segment is divided into the outer and inner layers, and the thickness of the outer layer is 100 mm (as shown in Figure 9(a)), which is thicker than cover concrete. The outer layer of the segment is the chloride penetrated part, where the strength and elastic modulus of the concrete are reduced due to chloride penetration. When steel bars there begin to rust, it bears the dual action of steel bar corrosion-induced force and concrete strength loss. The thickness of the inner layer is 250 mm (as shown in Figure 9(a)), where the seawater has not arrived. Since the carbonization does not reduce concrete strength, the steel bar corrosion-induced force is the only action on the outer layer.

The durability damage and performance degradation of subsea shield tunnel segments is mathematically a highly nonlinear problem, which is difficult to characterize this process relying on theory analysis. The model test method consumes a great deal of manpower and material resources, and the steel bar corrosion rate and characteristics obtained by accelerated corrosion test usually differ greatly from the actual situation. Thus, in this paper, the performance degradation process of the subsea shield tunnel segment is systematically investigated by XFEM on the Abaqus platform. Figure 9 demonstrates the numerical model. The model uses structured quadrilateral mesh and plane strain elements. The analysis steps are set to 23,871 with each step representing one day, in reality, to simulate the steel bar corrosion for 65.4 years. Adding the service time of 34.6 years before corrosion achieves 100 years so as to compute until the tunnel structure reaches its design reference period (service lifetime), namely 100 years. According to the test results of mechanical properties of C50 segment concrete in Section 2, the mechanical parameters of chloride penetrated concrete (i.e., chlorine-corroded saturated concrete) were given to the outer layer of the segment, while the mechanical parameters of uncorroded concrete were given to the inner layer so as to reflect the concrete strength difference of the outer and inner layers of the segment caused by chloride penetration.

The XFEM model for the whole segment is established with the combined stress-energy-based fracture criterion, specifically, damage for traction-separation law based on maximum principal stress damage initiation criteria and energy-based damage evolution law, and the fracture energy is set at 150 N/m according to literature [19]. The mechanical parameters of the segment concrete for the inner and outer layers are shown in Table 4.

The model boundary conditions are illustrated in Figure 9. The left and right boundaries of the segment are articulated. In the model, some holes with the same diameter and locations as the steel bars are used to represent the steel

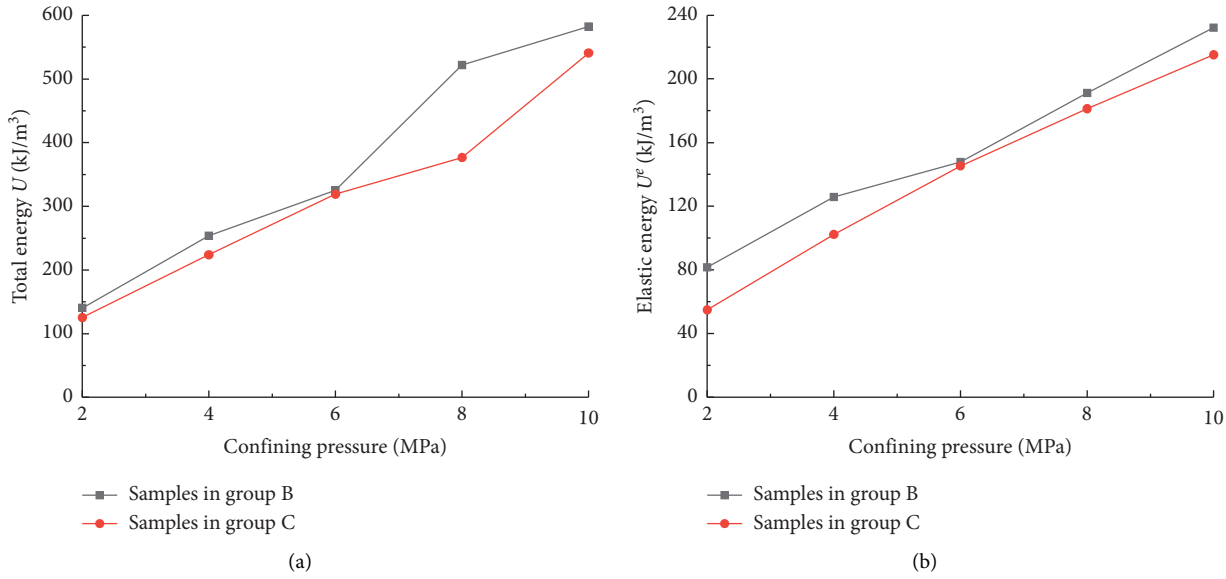

Figure 8: Curves of total energy and elastic energy of group B and group C samples changing with confining pressure at the peak stress point.

Table 3: Geometric dimensions of the K-block.

External diameter (mm)	Internal diameter (mm)	External boundary length (mm)	Internal boundary length (mm)	Segment thickness (mm)	Cover thickness (mm)	Steel bar spacing (mm)	Steel bar diameter (mm)
6,200	5,500	1,163	1,031	350	50	200	20

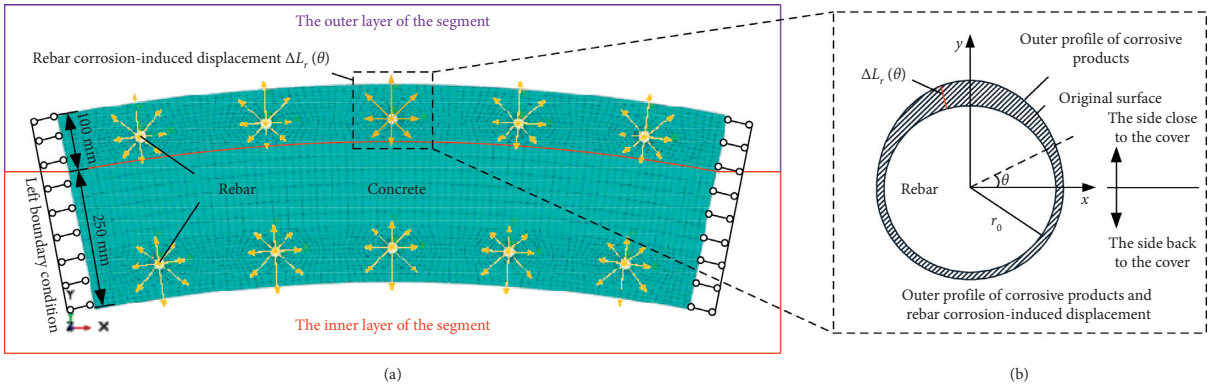

Figure 9: Numerical model of K-block: (a) outer and inner layer of the segment model and the boundary conditions and (b) outer profile of steel bar corrosive products.

Table 4: Mechanical parameters of segment concrete for the inner and outer layers.

Segment parts	Elasticity modulus (GPa)	Poisson's ratio	Fracture energy (N/m)	Viscosity
Outer layer	20.709	0.2	150	$1e-5$
Inner layer	38.928	0.2	150	$1e-5$

bars in the real segment. The radial corrosion-induced displacement is applied to each hole to simulate the expansion induced by the steel bar corrosion products. This method is the closest to reality and most commonly used [20, 21]. The corrosion-induced displacement is fitted by a nonuniform corrosion model whose outer profile of corrosive products is illustrated in Figure 9(b) [20, 22, 23]. In Figure 9(b), r_0 is the original radius of the steel bar. The outer profile of corrosive products has the shape of a half ellipse at the side close to the cover ($0 \le \theta \le \pi$), while back to the cover

($\pi \le \theta \le 2\pi$), it shows a semicircle. It is evident that the steel bar corrosion-induced displacement ΔL_r is a function of θ. In this paper, Geng's prediction model of steel bar corrosion-induced displacement is employed to calculate ΔL_r [24]. The relevant parameter values for computing steel bars corrosion-induced displacement are shown in Table 5. It is calculated that when steel bars corrode for 65.4 years, the expressions of ΔL_r for outer and inner steel bars under the polar coordinate are given as follows:

$$\Delta L_{r-\text{out}}(\theta) = \begin{cases} \dfrac{0.011799}{\sqrt{1.2996\cos^2\theta + 1.071225\sin^2\theta}} - 0.01, & 0 \le \theta \le \pi, \\ 0.00035, & \pi \le \theta \le 2\pi, \end{cases} \tag{6}$$

$$\Delta L_{r-\text{in}}(\theta) = \begin{cases} \dfrac{0.012331}{\sqrt{1.3924\cos^2\theta + 1.092025\sin^2\theta}} - 0.01, & 0 \le \theta \le \pi, \\ 0.00045, & \pi \le \theta \le 2\pi. \end{cases} \tag{7}$$

The continuous steel bar corrosion-induced displacements are applied to the outer and inner steel bar holes in accordance with formulas (6) and (7), respectively. Then the whole model should be selected as the XFEM enriched area, so that concrete cracking is caused only by the action of the displacement and the cracks can propagate to any position according to its cracking path.

3.2. Analysis of Numerical Results of Subsea Shield Tunnel Segment Deterioration. Based on the aforementioned XFEM model, the durability damage and performance degradation of the lining segment are obtained. The degradation characteristics of the segment at the beginning of steel bar corrosion are shown in Figure 10. At this time, there is a radial outward displacement around each steel bar, and the displacement is manifested that the side close to the cover is much larger than the side back to the cover, which meets the characteristics of the corrosion-induced displacement boundary conditions. The maximum principal stress of the concrete around the steel bars is positive, so the concrete is under tension. Moreover, the stress concentration at the shoulder of each steel bar is the highest.

With the increase of corrosion time, the steel bar corrosion-induced displacement gradually increases. After 60 days of corrosion, as shown in Figure 11(a), cracks initiate in the concrete around the outer steel bars; the concrete around the inner steel bars has not been cracked; and the cracks occur in the area where the tensile stress is most concentrated (Figure 10(b)). It indicates that the concrete does not crack immediately, this is because the stress caused by the corrosion displacement is small in the initial stage and does not reach the tensile limit of the concrete. So it needs to take some more time for corrosion to cause cracks initiation. Moreover, Figure 9(b) demonstrates that the tensile stress at the cracking area is still the largest even though the crack has initiated, which is because the cracks are too small to release the excessive stress.

After 120 days of corrosion, with the corrosion amount of steel bars continuing to increase, the outer crack continues to extend, and the concrete around the inner steel bars just begins to crack initiation, as shown in Figure 12(a). When the crack length increases rapidly, the originally concentrated stress close to the crack is released to a certain extent so that the stress of the concrete close to the cracks decreases slightly compared with that far away from the cracks, as shown in Figure 12(b).

As shown in Figure 13, when corrosion lasts for one year, the cracks around the outer steel bars propagate rapidly, and the length of the cracks increases greatly, which results in a serious damage to the outer layer of the segment. After the outer cracks propagate for a certain length, the concrete around the inner steel bars continues to crack (Figure 13(a)). Although the corrosion-induced displacement of the inner steel bars is slightly larger than that of the outer steel bar, the inner layer cracks later, indicating that the reason comes from the different concrete materials of the inner and the outer layer. The concrete around the outer steel bars has been weakened by chloride penetration, while for the inner layer, the concrete strength has not reduced, which further demonstrates that concrete strength loss caused by chloride penetration can accelerate the initiation of corrosion-induced cracks and accelerate the early-stage damage of segments.

Figure 14 shows the degradation characteristics of segments after 5 years of steel bars corrosion. It can be seen from Figure 14 that both outer and inner rust expansion cracks have expanded greatly, and the cracking area presents the wedge-shaped characteristics towards the side of the protective layer, in which the outer side faces the outer protective layer and the inner side faces the inner protective layer. The cracks propagated for a long distance and basically extended to the concrete boundary but did not penetrate the boundary.

According to Figure 15, when the steel bars of the segments corrosion reaches 10 years, the propagation speed of the outer cracks slows down; the propagation strength of the inner cracks gradually catches up with the outer cracks;

Table 5: Relevant parameter values for computing steel bar corrosion-induced displacement.

Water-cement ratio	Annual average temperature (°C)	Steel bar density (kg/m^3)	Outside O_2 concentration (mol/m^3)	Inside O_2 concentration (mol/m^3)	Outside relative humidity	Inside relative humidity
0.36	21	786.2254	1.09	8.67	1	0.78

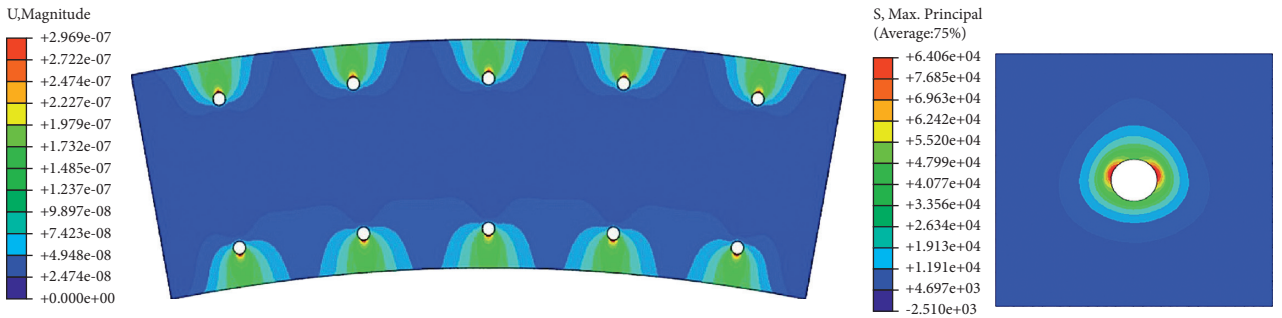

(a) (b)

Figure 10: Degradation characteristics of the segment after 1 day of steel bar corrosion: (a) the displacement cloud during cracking and (b) the maximum principal stress cloud during cracking.

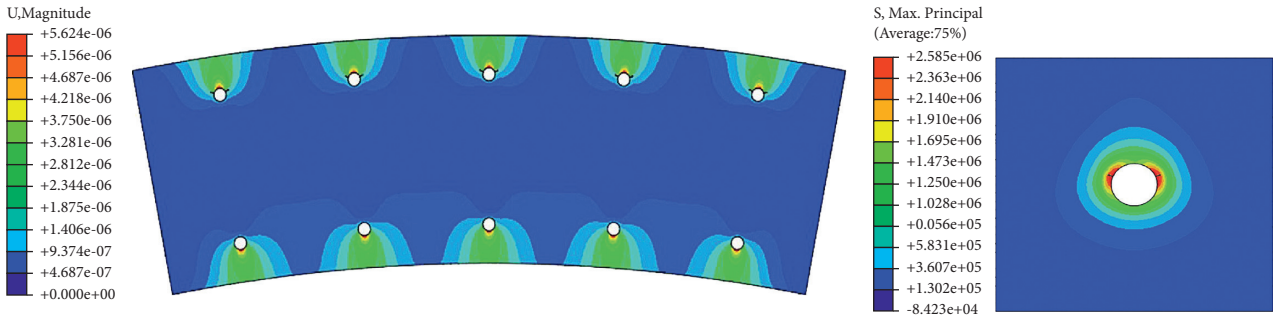

(a) (b)

Figure 11: Degradation characteristics of the segment after 60 days of steel bar corrosion: (a) the displacement cloud during cracking and (b) the maximum principal stress cloud during cracking.

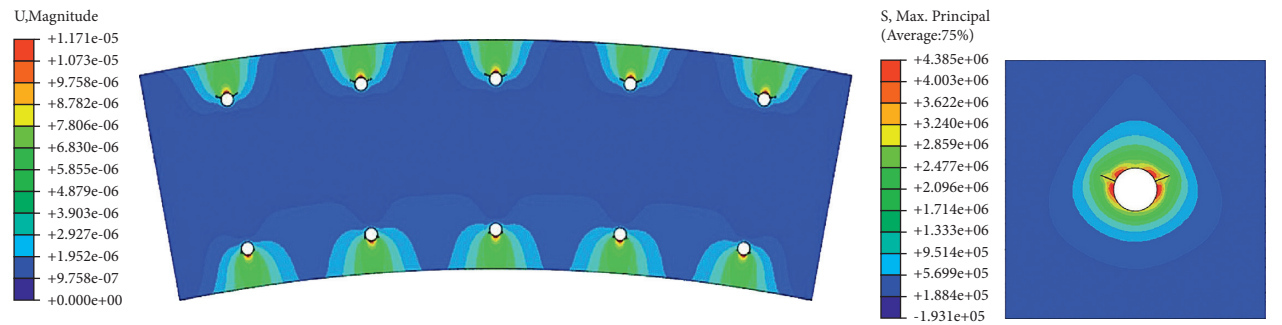

(a) (b)

Figure 12: Degradation characteristics of the segment after 120 days of steel bar corrosion: (a) the displacement cloud during cracking and (b) the maximum principal stress cloud during cracking.

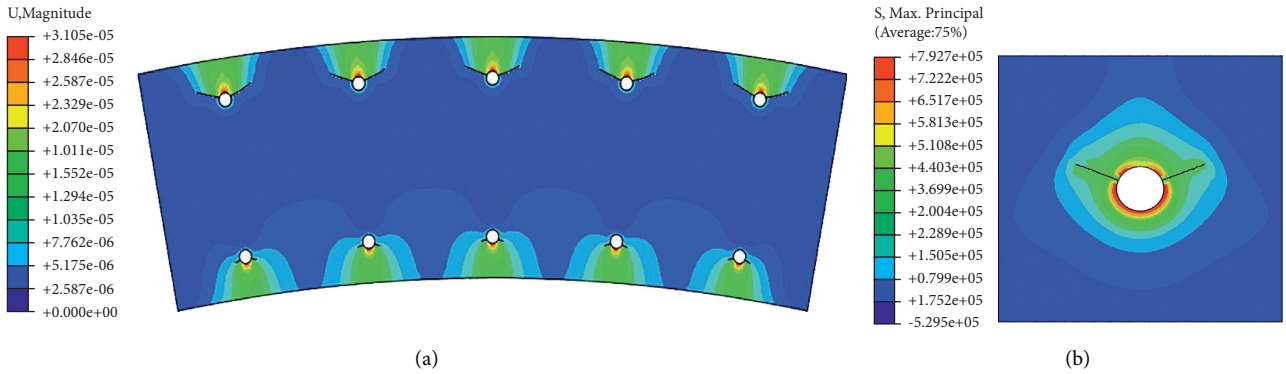

FIGURE 13: Degradation characteristics of the segment after 1 year of steel bar corrosion: (a) the displacement cloud during cracking and (b) the maximum principal stress cloud during cracking.

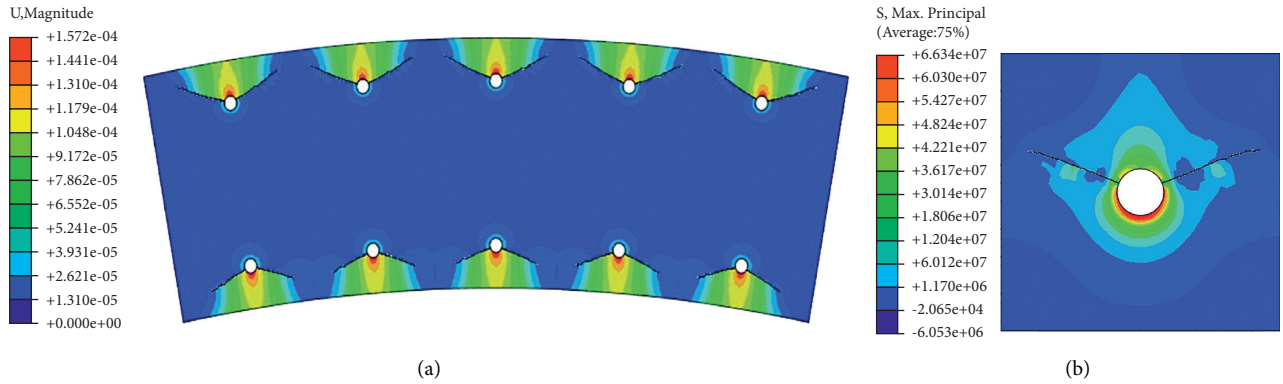

FIGURE 14: Degradation characteristics of the segment after 5 years of steel bar corrosion: (a) the displacement cloud during cracking and (b) the maximum principal stress cloud during cracking.

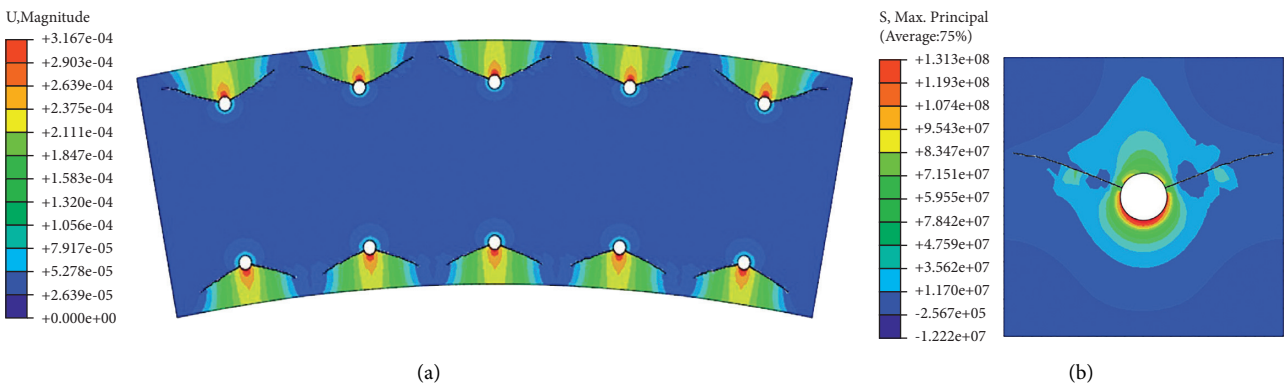

FIGURE 15: Degradation characteristics of the segment after 10 years of steel bar corrosion: (a) the displacement cloud during cracking and (b) the maximum principal stress cloud during cracking.

and the length of inner and outer cracks is almost the same. The reason can be explained by Hooke's law. According to the test results in Section 2, the elastic modulus of the concrete segment not eroded by seawater is 38.928 GPa, while the elastic modulus of the concrete after seawater erosion is 22.322 GPa. The elastic modulus of the not eroded part of the inner ring of the segment is much larger than that of the outer ring, and the applied displacement of the inner ring is slightly larger than that of the outer side. According to Hooke's law, under the condition of large rust expansion displacement and large elastic modulus of concrete, the rust expansion stress of inner ring concrete is greater than that of the outer ring; the inner crack propagates rapidly.

When corrode for 20 years, the cracks in both the inner and outer layers have extended greatly (Figure 16). During the process, the length of the inner cracks gradually exceeds

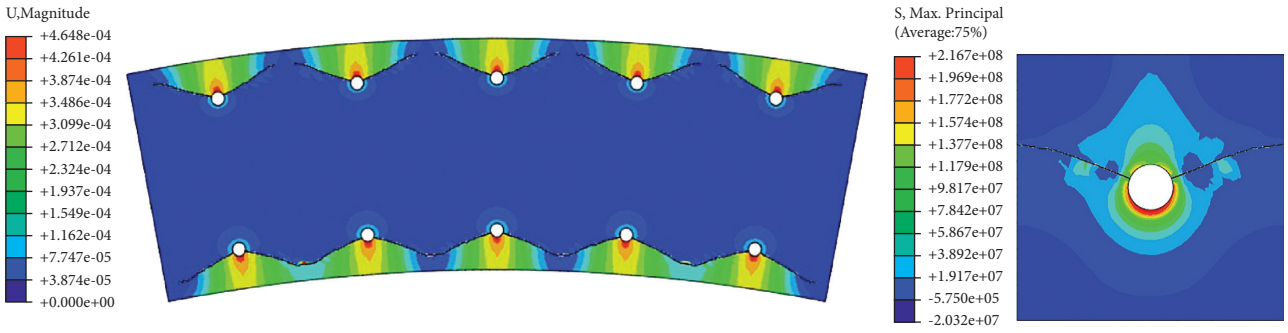

FIGURE 16: Degradation characteristics of the segment after 20 years of steel bar corrosion: (a) the displacement cloud during cracking and (b) the maximum principal stress cloud during cracking.

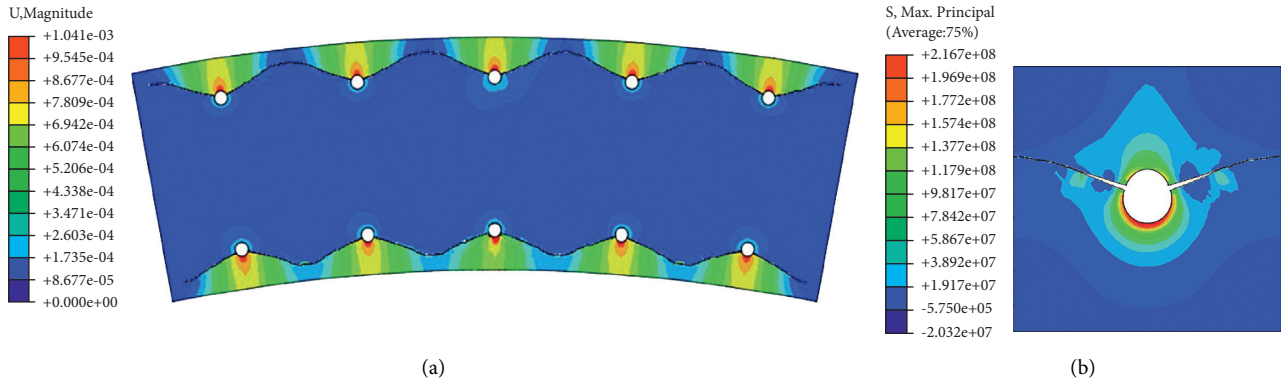

FIGURE 17: Degradation characteristics of the segment after 20 years of steel bar corrosion: (a) the displacement cloud during cracking and (b) the maximum principal stress cloud during cracking (deformation amplification factor is 10).

that of the outer cracks, and the inner cracks initiating from different steel bars coalesce with each other and form a continuous failure surface, causing great serious damage to the segment. Although the outer cracks initiate earlier than the inner cracks, the inner cracks coalesce to fail the cover first. The reason can be explained based on Hook's law. The elastic modulus of the uncorroded inner layer concrete is 38.928 GPa, while that of the outer layer concrete after chloride penetration is 20.709 GPa, so the elastic modulus of the inner layer concrete is much larger than that of the outer layer concrete. According to Hooke's law, under the conditions of larger corrosion-induced displacement and larger elastic modulus, the tensile stress acting on the inner layer concrete should be greater than that acting on the outer layer concrete. Under the action of the large tensile stress, the cracks propagate more rapidly.

Figure 17 shows the effect diagram of enlarging the crack width by 10 times when the steel bar is corroded for 20 years. It can be seen that the crack width near the surface of the steel bar is larger, and the crack width decreases with the increase of the distance. With the further increase of corrosion time and after the coalescence of the inner cracks, each outer crack continues to propagate and coalesces with the adjacent crack approximately at the midpoint of the two adjacent steel bars to form a continuous failure surface. The coalescence of the cracks causes the inner and outer layers of the segment to form a peeling surface; the whole concrete cover has a large displacement (Figure 17(a)) so that the whole cover is pushed and separated from the original segment; and it appears as a whole lamellar exfoliation with the outer cover moving up and inner cover moving down, reaching the final state of segment performance degradation.

From the comprehensive analysis of the above figures, in terms of the entire performance degradation evolution process of the initiation, propagation, and coalescence of the corrosion-induced cracks, the propagation speed of the inner and outer cracks show a certain regularity. As the length of the cracks continues to increase, the propagation speed of corrosion-induced cracks appears to be fast first and then slow. This phenomenon can be explained according to Figure 17. In Figure 17(a), concrete cracking makes the displacement fields on both sides of the crack appear severely discontinuous, which manifests as the difference of displacement magnitude of the concrete on both sides of the crack. As the corrosion-induced displacement only acts on the interface between the steel bar and the surrounding concrete, the closer the crack is to the steel bar, the greater the difference is, and the farther the smaller difference is, as shown in Figure 17(a). When it comes to crack width, the crack is relatively wider near the steel bar, and the farther it is, the narrower it is, and concrete cracks are the farther from the steel bars; the tensile stress of cracks is smaller (Figure 17(b)). Therefore, the farther away from the

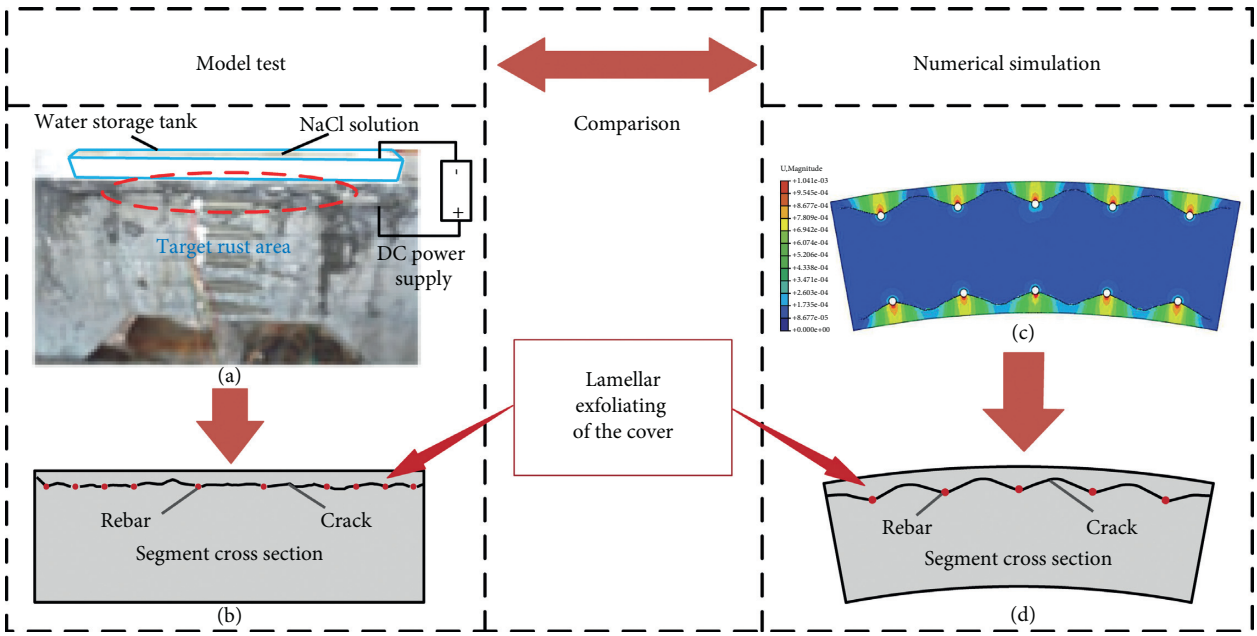

Figure 18: Comparison of segment failure patterns between model test and numerical simulation: (a) experimental setup and failure characteristics of the model test, (b) failure pattern observed from model test, (c) the displacement cloud when segments failure, and (d) failure pattern observed from numerical simulation.

Table 6: Comparison of parameters between model test and numerical simulation.

Research method	Thickness of the segment (mm)	Thickness of the cover (mm)	Strength grade of concrete	Diameter of main steel bar (mm)	Steel bar spacing (mm)	Type of main steel bar
Model test	350	50	C50	20	190	HRB335
Numerical simulation	350	50	C50	20	200	HRB400

steel bar, the smaller the difference between the two sides of the crack in the displacement field, the more difficult to propel concrete cracking, the more time it takes for accumulating the tensile stress until tensile strength, and the slower the crack propagation.

4. Discussion

Liu designed a straight beam segment specimen instead of the prototype curved segment to make a simplified segment model as shown in Figure 18(a) [25]. The area around the outer steel bars in Figure 18(a) is selected as the target rust area, and a water tank containing NaCl solution on top of the target rust area is constructed. The electrochemical-accelerated corrosion method is used to simulate the performance degradation process and failure pattern of the subsea shield tunnel segment. In this model test, the segment geometry, concrete material, and segment service environment are very similar to those of the numerical model in this paper, and the comparison of both is illustrated in Table 6. As shown in Figure 18(b), in the model test, the steel bar corrosion-induced cracks in the target rust area do not penetrate the cover vertically but extend approximately parallel to cover and connect with the adjacent cracks until the cover exfoliated as a whole lamella. The whole lamellar exfoliation characteristic of the cover at the final state of segment performance degradation acquired from the numerical simulation is consistent with the failure pattern observed from the model test (shown in Figures 18(c) and 18(d)), which verifies the credibility and reasonability of the numerical simulation results.

5. Conclusions

In this paper, the systematical experimental and numerical investigations into performance degradation of subsea shield tunnel segment induced by concrete strength loss and steel bar corrosion are carried out, and the following conclusions can be drawn:

(1) Chloride penetration weakens the peak strength and elastic modulus of the segment concrete significantly. After chloride penetration, the strength of segment concrete decreased by 42%, and the elastic modulus decreased by 46.1%. The average of the ratio of dissipated energy to the total energy of dry concrete is much smaller than that of water saturated concrete and chlorine solution saturated concrete; the total energy and elastic strain energy of water saturated concrete samples are slightly larger than that of chlorine solution saturated concrete samples. Chloride penetration reduces the energy storage

capacity of concrete, and the ability to resist damage is weakened.

(2) When steel bars corrode for 60 days, the cracks initiate in the concrete around the outer steel bars. When corrode for 120 days, the outer cracks continue to extend, and the concrete around the inner steel bars just begins to crack initiation. When corrode for 5 years, the cracks propagated for a long distance and basically extended to the concrete boundary but did not penetrate the boundary. When corrode for 10 years, the propagation strength of the inner cracks gradually catches up with the outer cracks, and the length of the inner and outer cracks is almost the same. When corrode for 20 years, the length of the inner cracks gradually exceeds that of the outer cracks, and the inner cracks initiating from different steel bars coalesce with each other and form a continuous failure surface, causing great serious damage to the segment.

(3) The inner and outer layers of the segment divided according to the chloride penetration depth show different performance degradation characteristics. For the inner layer, it manifests as steel bar corrosion-induced concrete cracking; but for the outer layer, concrete strength loss should also be considered. Due to the difference in concrete strength, for the outer layer, the evolution processes of steel bar corrosion-induced cracks show the characteristics of early initiation, slow propagation, and late coalescence; and those for the inner layer have the characteristics of late initiation, rapid propagation, and early coalescence. During the whole process, the propagation speed of the inner and outer cracks appears to be fast first and then slow.

(4) In the model test, the segment geometry, concrete material, and segment service environment are very similar to those of the numerical model in this paper; the steel bars corrosion-induced cracks in the target rust area do not penetrate the cover vertically but extend approximately parallel to cover and connect with the adjacent cracks until the cover exfoliated as a whole lamella. The final state of segment performance degradation after crack coalescence presents the characteristics of whole lamellar exfoliation of the concrete cover, which coincides well with the previous researchers' observation of segment degradation characteristics of shield tunnel through the model test.

Data Availability

The data used to support the findings of this study are available from the corresponding author upon request.

Conflicts of Interest

The authors declare that there is no conflict of interest regarding the publication of this paper.

Authors' Contributions

Jiaqi Guo and Chong Xu conceived, designed, and performed the study. Bo Peng, Jinhai Lin, and Yuan Qian conducted relevant experiments and analyzed the data used in the paper. Weiling Yang wrote and rearranged the paper. The authors have read and approved the final published manuscript.

Acknowledgments

This research was funded by the National Natural Science Foundation of China (No. 51778215), the Scientific and Technological Development Projects of FSDI [17–25], and the Shaanxi Key Scientific and Technological Innovation Team Plan (2015KCT-01).

References

[1] C. He and K. Feng, "Review and prospect of structure research of underwater shield tunnel with large cross-section," *Journal of Southwest Jiaotong University*, vol. 64, pp. 1–11, 2011.

[2] J. Sun, *Collected Works of Academician Sun Jun in His Sixty-Five Years of Teaching*, Tongji University Press, Shanghai, China, 2016.

[3] S. Guzmán, J. C. Gálvez, and J. M. Sancho, "Cover cracking of reinforced concrete due to rebar corrosion induced by chloride penetration," *Cement and Concrete Research*, vol. 41, no. 8, pp. 893–902, 2011.

[4] P. Thoftchristensen, "Corrosion and cracking of reinforced concrete," *ACI Materials Journal*, vol. 106, pp. 26–36, 2004.

[5] S. Abbas and M. L. Nehdi, "Mechanical behavior of RC and SFRC precast tunnel lining segments under chloride ions exposure," *Journal of Materials in Civil Engineering*, vol. 30, no. 4, pp. 1–13, 2018.

[6] R.-R. Yin, J. Hu, and Y. Liu, "The degradation of macro-mechanical properties of shield tunnel segments," *Modern Physics Letters B*, vol. 32, pp. 1–7, 2018.

[7] X.-X. Kong, C.-C. Xia, Y.-L. Qiu, and X.-L. Kuang, "Effect of lining degradation on deformation behavior of underwater shield tunnel," *Highway Engineer*, vol. 37, pp. 26–31, 2012.

[8] M. Lei, L. Peng, and C. Shi, "An experimental study on durability of shield segments under load and chloride environment coupling effect," *Tunnelling and Underground Space Technology*, vol. 42, pp. 15–24, 2014.

[9] J. W. Bao, Z. J. Zhuang, P. Zhuang, J. N. Wei, S. Gao, and T. J. Zhao, "Research progress on chloride resistance of environmental concrete in marine tidal area based on similarity," *Materials Reports*, vol. 35, no. 7, pp. 7087–7095, 2021.

[10] K. Feng, S. Liu, C. He et al., "Experiment study on chloride corrosion deterioration of load-bearing concrete segment," *Advances in Structural Engineering*, vol. 3, pp. 1–11, 2018.

[11] Z.-S. He, S. Supasit, M. Akiyama, and D. M. Frangopol, "Life-cycle reliability-based design and reliability updating of reinforced concrete shield tunnels in coastal regions," *Structure and Infrastructure Engineering*, vol. 16, no. 4, pp. 726–737, 2020.

[12] Z. Li, H. M. Chen, F. X. Sun, and X. D. Hu, "Tests on structure behavior's degradation of shield tunnel lining in chloride erosion," *Chinese Journal of Underground Space and Engineering*, vol. 5, pp. 1902–1109, 2009.

[13] Q. Li, H. Yu, H. Ma, S. Chen, and S. Liu, "Test on durability of shield tunnel concrete segment under coupling multi-factors,"

The Open Civil Engineering Journal, vol. 8, no. 1, pp. 451–457, 2014.

[14] Y. L. Li, X. H. Liu, Z. Q. Zhang, and Y. Chen, "Study on performance deterioration law of tunnel lining structure under steel corrosion based on thermal - mechanical coupling analysis," *Railway Standard Design*, vol. 66, no. 2, pp. 1–9, 2021.

[15] H. P. Xie, Y. Ju, and L. Y. Li, "Criteria for strength and structural failure of rocks based on energy dissipation and energy release principles," *Chinese Journal of Rock Mechanics and Engineering*, vol. 24, no. 17, pp. 3003–3010, 2005.

[16] Y. Wang and F. Cui, "Energy evolution mechanism in process of sandstone failure and energy strength criterion," *Journal of Applied Geophysics*, vol. 154, pp. 21–28, 2018.

[17] T. Cheewaket, C. Jaturapitakkul, and W. Chalee, "Concrete durability presented by acceptable chloride level and chloride diffusion coefficient in concrete: 10-year results in marine site," *Materials and Structures*, vol. 47, no. 9, pp. 1501–1511, 2014.

[18] Y. Qian, "Macro-microscopic study on deterioration mechanism of lining structure of subsea shield tunnel in commission," Dissertation, Hennan Polytechnic University, Jiaozuo, China, 2020.

[19] L. Li, "Extended finite element method (XFEM)-research of crack growth in concrete structure," Dissertation, Chongqing Jiaotong University, Chongqing, China, 2014.

[20] E. Chen and C. K. Y. Leung, "Finite element modeling of concrete cover cracking due to non-uniform steel corrosion," *Engineering Fracture Mechanics*, vol. 134, pp. 61–78, 2015.

[21] J. Zhang and M. M. S. Cheung, "Modeling of chloride-induced corrosion in reinforced concrete structures," *Materials and Structures*, vol. 46, no. 4, pp. 573–586, 2013.

[22] X.-D. Cheng, L.-F. Sun, Z.-F. Cao, and X.-J. Zhu, "Cracking process analysis of concrete cover caused by non-uniform corrosion," *Journal of Chinese Society for Corrosion and Protection*, vol. 35, pp. 257–264, 2015.

[23] Y. S. Ji, Y. S. Yuan, J. L. Shen, S. P. Lai, and L. Qin, "Model for predicting steel corrosion rates of concrete rebar over time," *Journal of China University of Mining and Technology*, vol. 40, pp. 339–344, 2011.

[24] O. Geng, Y. Yuan, and F. Li, "Study on the corrosion rate of steel bars in concrete under high humidity conditions," *International Journal of Modelling, Identification and Control*, vol. 7, no. 2, pp. 155–159, 2009.

[25] S. J. Liu, C. He, K. Feng, and Z. L. An, "Research on corrosion deterioration and failure process of shield tunnel segments under loads," *China Civil Engineering Journal*, vol. 51, pp. 120–128, 2018.